GDCh

Research Article

Angewandte
Chemie
International Edition
www.angewandte.org

VIP **Molecular Recognition** *Very Important Paper*

Detection of Tumor-Associated Autoantibodies in the Sera of Pancreatic Cancer Patients Using Engineered MUC1 Glycopeptide Nanoparticle Probes

Francisco Corzana[+],* Alicia Asín[+], Ander Eguskiza[+], Elisa De Tomi[+],
Alfonso Martín-Carnicero, María P. Martínez-Moral, Vincenzo Mangini, Francesco Papi,
Carmen Bretón, Paula Oroz, Laura Lagartera, Ester Jiménez-Moreno, Alberto Avenoza,
Jesús H. Busto, Cristina Nativi, Juan L. Asensio, Ramón Hurtado-Guerrero,
Jesús M. Peregrina, Giovanni Malerba,* Alfredo Martínez,* and Roberto Fiammengo*

Abstract: Pancreatic cancer is one of the deadliest cancers worldwide, mainly due to late diagnosis. Therefore, there is an urgent need for novel diagnostic approaches to identify the disease as early as possible. We have developed a diagnostic assay for pancreatic cancer based on the detection of naturally occurring tumor associated autoantibodies against Mucin-1 (MUC1) using engineered glycopeptides on nanoparticle probes. We used a structure-guided approach to develop unnatural glycopeptides as model antigens for tumor-associated MUC1. We designed a collection of 13 glycopeptides to bind either SM3 or 5E5, two monoclonal antibodies with distinct epitopes known to recognize tumor associated MUC1. Glycopeptide binding to SM3 or 5E5 was confirmed by surface plasmon resonance and rationalized by molecular dynamics simulations. These model antigens were conjugated to gold nanoparticles and used in a dot-blot assay to detect autoantibodies in serum samples from pancreatic cancer patients and healthy volunteers. Nanoparticle probes with glycopeptides displaying the SM3 epitope did not have diagnostic potential. Instead, nanoparticle probes displaying glycopeptides with high affinity for 5E5 could discriminate between cancer patients and healthy controls. Remarkably, the best-discriminating probes show significantly better true and false positive rates than the current clinical biomarkers CA19-9 and carcinoembryonic antigen (CEA).

[*] Prof. Dr. F. Corzana,[+] Dr. A. Asín,[+] C. Bretón, Dr. P. Oroz,
Dr. E. Jiménez-Moreno, Prof. Dr. A. Avenoza, Prof. Dr. J. H. Busto,
Prof. Dr. J. M. Peregrina
Departamento de Química, Instituto de Investigación en Química
(IQUR), Universidad de La Rioja, Logroño, 26006 Logroño, (Spain)
E-mail: francisco.corzana@unirioja.es

A. Eguskiza,[+] Prof. Dr. R. Fiammengo
Department of Biotechnology, University of Verona
Strada Le Grazie 15, 37134 Verona, (Italy)
E-mail: roberto.fiammengo@univr.it

Dr. E. De Tomi,[+] Prof. Dr. G. Malerba
Department of Neurosciences, Biomedicine and Movement Scien-
ces, GM Lab, University of Verona, 37134 Verona, (Italy)
E-mail: giovanni.malerba@univr.it

Dr. M. P. Martínez-Moral, Dr. A. Martínez
Oncology Area, Angiogenesis Group, Center for Biomedical
Research of La Rioja (CIBIR), Logroño, 26006 Logroño, (Spain)
E-mail: amartinezr@riojasalud.es

Dr. A. Martín-Carnicero
Medical Oncology Department, Hospital San Pedro
Logroño, 26006 Logroño, (Spain)

Dr. M. P. Martínez-Moral
Wadsworth Center, New York State Department of Health, Biggs
Laboratory, Corning Tower, ESP. 12201, Albany, NY, (USA)

Dr. V. Mangini, Prof. Dr. R. Fiammengo
Center for Biomolecular Nanotechnologies@UniLe, Istituto Italiano
di Tecnologia (IIT), 73010 Arnesano, Lecce (Italy)

Dr. F. Papi, Prof. Dr. C. Nativi
Department of Chemistry "Ugo Schiff", University of Florence
50019 Sesto Fiorentino (FI), (Italy)

Dr. L. Lagartera
Servicios de Interacciones Biofísicas, Instituto de Química Médica
(CSIC), C/Juan de la Cierva, 3, 28006 Madrid (Spain)

Dr. J. L. Asensio
Departamento de Química Bio-Orgánica, Instituto de Química
Orgánica General (IQOG-CSIC), Consejo Superior de Investiga-
ciones Científicas (CSIC), 28006 Madrid (Spain)

Dr. R. Hurtado-Guerrero
Institute of Biocomputation and Physics of Complex Systems,
University of Zaragoza, 50018 Zaragoza (Spain),
and
Copenhagen Center for Glycomics, Department of Cellular and
Molecular Medicine, University of Copenhagen, Copenhagen DK-
2200(Denmark),
and
Fundación ARAID, 50018, Zaragoza, (Spain)

[+] These authors contributed equally to this work.

Introduction

Pancreatic cancer (PC) is the fourteenth most common cancer globally and the seventh leading cause of cancer-related deaths.[1] The high lethality of this disease is a consequence of the late detection of this tumor.[2] In fact, most patients are diagnosed with locally advanced or metastatic disease, which renders them ineligible for surgery. The 5-year relative survival rate according to the latest statistical data in the US is only 11 % for all disease stages combined.[3] In particular it is around 40 % for localized-stage disease at diagnosis but it drops to 14 % for regional- and to 3 % for distant-stage disease at diagnosis. These dismaying numbers highlight the importance for early detection of PC as the most effective way to improve survival.

In the clinical management of patients with PC, carbohydrate antigen 19–9 (CA19-9, a tetra saccharide also known as sialyl-Lewis A) is the most routinely used biomarker.[4] CA 19–9 is considered a good diagnostic marker only in symptomatic patients with sensitivity of 72 % and specificity of 86 % resulting from the most recent meta-analysis of 79 studies conducted between 2002 and 2022 on a total of 20,991 patients.[5] CA19-9 is not recommended for screening the general population for PC but only for monitoring of benign pancreatic diseases and the screening of high PC risk individuals with a family history.[5–6] To date, no biomarker or panel of biomarkers with sufficient diagnostic accuracy has been approved for the early diagnosis of PC.[2b] Therefore, finding alternative, possibly more sensitive and specific, biomarkers is crucial to improve early detection, allowing for prompt medical intervention and higher patient survival rates.

One appealing possibility would be the exploitation of circulating tumor-associated autoantibodies because of their ready accessibility in serum samples.[2a,7] It is known that developing tumors produce tumor-associated antigens, which may elicit an immune response as a consequence of immunosurveillance.[8] Tumor-associated autoantibodies effectively represent a natural amplification mechanism and can be identified at a very early stage of the disease before tumor-associated antigens can be detected, thus being ideally suited for early diagnosis.[9] Unfortunately, despite strong interest in the application of autoantibodies as biomarkers,[8b] their exploitation for PC diagnosis is still missing in the current clinical practice.

In this work, we focus on the detection of autoantibodies against the tumor-associated form of Mucin-1 (TA-MUC1)[10] in the sera of PC patients. In healthy individuals, MUC1 is a heavily *O*-glycosylated protein expressed on the surface of epithelial cells. The large extracellular domain of MUC1, known as the *variable number of tandem repeats* domain, consists of 20–120 tandem repeats of 20 amino acids (AHGV**TS**APD**T**RPAPG**ST**APP) containing five *O*-glycosylation sites (in bold letters) with the first sugar being *N*-acetylgalactosamine (GalNAc).[11] In many types of epithelial cancer, including PC,[12] MUC1 is overexpressed and glycosylation is dramatically altered. Specifically, TA-MUC1 is decorated only with simple and truncated carbohydrates.[13] The occurrence of autoantibodies against TA-MUC1 was initially demonstrated using completely unglycosylated peptides[14] and recombinant protein portions,[15] as simplistic models of the heterogeneous nature of this tumor associated antigen. Yet, glycosylation plays a significant role in the 3D structure of TA-MUC1[10] and the use of unglycosylated antigen models may result in a failure to detect relevant tumor associated autoantibodies. Hence, Blixt, Clausen and co-workers have used arrays of glycopeptides to detect autoantibodies that specifically recognize glycosylated epitopes with varying degree of success.[16] Notably, MUC1 autoantibodies have been detected both in patients with malignant tumors as well as in healthy people with no history of cancer, which is currently interpreted as a consequence of acute inflammation events or viral infections.[17] This observation underlines the importance of using antigen models that specifically mimic tumor-associated epitopes of MUC1.

We hypothesize it would be possible to develop a diagnostic assay for PC by engineering artificial *O*-GalNAc glycopeptides to mimic a specific cancer epitope via a structure-based approach, starting from known antibody-antigen complexes. These unnatural glycopeptides would allow to detect subsets of autoantibodies that are truly associated with the tumor thereby allowing stratification of patients vs. healthy controls (Figure 1).

For the last several years, we have been investigating the binding of unnatural glycopeptides that mimic TA-MUC1 to monoclonal anti MUC1 antibodies.[18] The introduction of unnatural modifications in the glycopeptide epitope modulates and sometimes increases binding.[18b,c,e] We have also used unnatural glycopeptides to elicit a humoral immune response in mice and shown that the elicited antibodies cross-react with natural TA-MUC1.[18a,b,19] Finally, we and another group have reported preliminary data suggesting that unnatural MUC1 glycopeptides may be used to detect autoantibodies in prostate cancer[18c] and in breast cancer.[20]

In this work, we report on the development of a diagnostic assay for PC based on the detection of tumor-associated autoantibodies with (un)natural glycopeptides as model antigens for TA-MUC1, immobilized on the hydrophilic, poly(ethylene glycol)-based coating of gold nanoparticles (AuNPs). A small glycopeptide library was designed via structural analysis starting from the known X-ray structure of two TA-MUC1 monoclonal antibodies complexing MUC1 glycopeptides. The members of this library were synthesized, and their binding was assayed experimentally via surface plasmon resonance (SPR). Representative variants were subjected to extensive molecular dynamics (MD) simulations, which contributed to the understanding of the observed results. Then a dot-blot assay was established to verify the binding of these TA-MUC1 monoclonal antibodies to the model antigens immobilized on AuNPs nanoparticles (**AuNP1–14**). Finally, we analyzed the sera from a group of 20 PC patients and 20 age- and sex-matched healthy volunteers to evaluate the diagnostic potential of our dot-blot assay. We conducted a retrospective observational clinical study to determine which members of the nanoparticle library would provide case/control
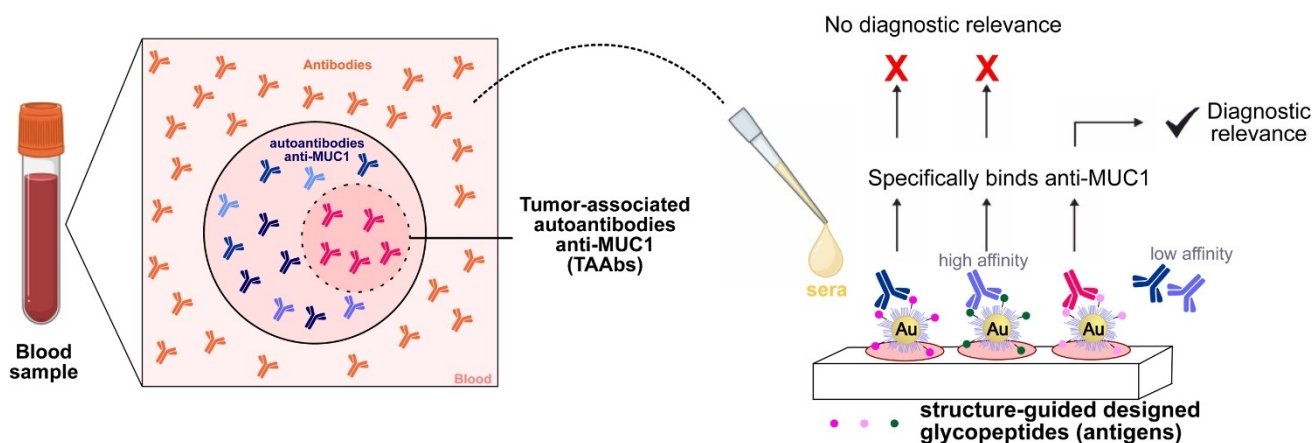
Figure 1. Diagnostic assay principle: designed unnatural glycopeptides are used as models of the TA-MUC1 antigen. A library of nanoparticle probes displaying these peptides is employed to detect anti-MUC1 autoantibodies in the sera of pancreatic cancer patients with each probe binding a different subset of autoantibodies. Only probes detecting tumor-associated autoantibodies have diagnostic relevance. Created with BioRender.com.

discrimination by binding antibodies in the plasma of patients and healthy volunteers. Our work shows that it is possible to exploit structurally engineered unnatural glycopeptides to develop a nanoparticle-based diagnostic assay that detects subsets of autoantibodies associated with the tumoral state. Remarkably, the presence of the GST*A epitope (where T* stands for the Tn antigen -α-O-GalNAc-Thr-) is demonstrated as an essential prerequisite for the specific detection of tumor-associated MUC1 autoantibodies.

Results and Discussion

Design and Synthesis of a Library of TA-Muc1 Antigen Models

We designed a small library of TA-MUC1 antigen models, most of them being glycopeptides with unnatural modifications (Figure 2). The envisioned design strategy contemplates: 1) a putative advantage of using relatively short glycopeptides as antibody capture agents for assay convenience; 2) peptides that are GalNAc-glycosylated and contain a single well-established immunodominant regions within the variable number of tandem repeats domain of MUC1; and 3) the incorporation of unnatural chemical modifications to modulate antibody binding affinity thereby potentially altering the identification of subsets of autoantibodies. Our 14-member library comprises nine peptides whose sequences are only nine amino acids long and mimic a single epitope of either 5E5[21] or SM3[22] monoclonal antibodies, see below. This collection of short peptides includes: three unnatural glycopeptides and the natural counterpart to mimic the GST*A epitope (glycopeptides **1–4**); four unnatural glycopeptides and the natural counterpart to mimic the PDT*R epitope (glycopeptides **5–9**). Additionally, we included four full-length tandem repeat derivatives. Three of them display a single Tn (**10** and **11**) or two Tn antigens (**12**) at the same location of the short variants. The fourth

full-length glycopeptide contains the noncanonical amino acid (2S,3R)-3-hydroxynorvaline (Hnv) in the PDT*R region (**13**).[18a] Finally, we included in the library an unnatural Tn antigen mimic with a constraint bicyclic structure (**14**).[23] This compound was previously shown to elicit a specific immune response in mice when conjugated to CRM_{197} (Cross Reactive Material 197) as a carrier protein.[24] The elicited immune response was directed against the natural Tn antigen as demonstrated by staining of human breast cancer cells. Unnatural glycopeptides (**2–4**, **6–9**, and **13**) were devised following a structure-guided approach based on the X-ray structures of two mouse monoclonal antibodies – 5E5 and SM3 – in complex with glycopeptides comprising the GST*A[25] and PDT*R[18f] sequences, respectively. These two antibodies were selected according to several criteria. First, both can discriminate with high specificity the tumor-associated form of MUC1 from the healthy tissue variant. Second, they are characterized by distinct epitopes both affected by glycosylation: in case of 5E5, glycosylation of Thr is necessary for binding,[21] while SM3 binds a peptide epitope and accommodates Tn[18f] but not larger *O*-glycans (core2).[26] Third, although both antibodies were raised in mice, it has been shown that the same molecular structures used for mice immunization are immunogenic in humans.[17a,27]

With these points in mind, the available structural information was used to introduce unnatural modifications that possibly favor binding of the glycopeptides to these two monoclonal antibodies and to putative autoantibodies with similar reactivity. More specifically, our design efforts aimed at modulating well-conserved CH/π interactions observable in crystallographic complexes. For instance, the fluorine atom in Pro of compound **9** is expected to strengthen the CH/π interaction between this residue and Trp91[L] by polarizing the C–H moieties of this proline that interact with the aromatic ring of the tryptophan, in agreement with previous studies.[18c] Similarly, variant **3** equipped with a *N*-propionyl group attached to the sugar moiety is expected to establish
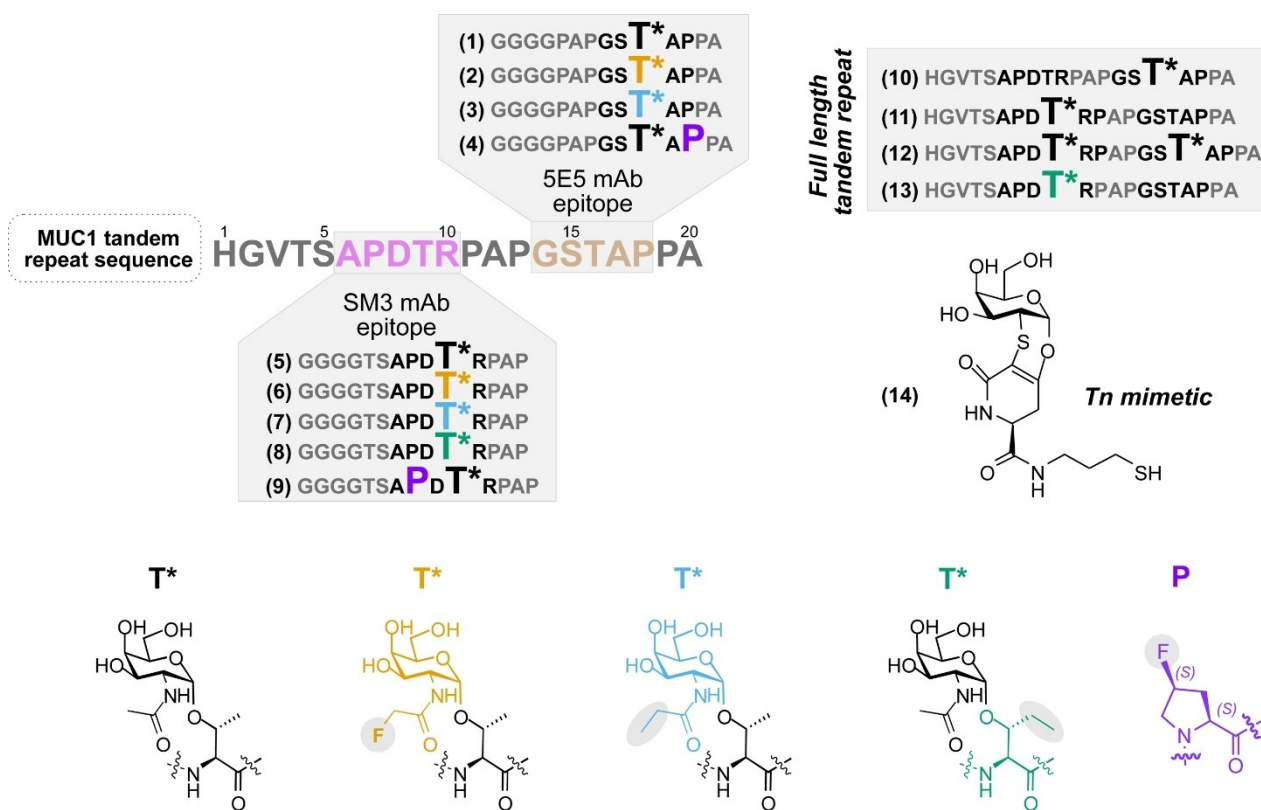
Figure 2. Structures of the tumor-associated MUC1 (TA-MUC1) model antigens used in this work.

stronger CH/π interactions with H50^H in the complex with 5E5 antibody due to the anticipated closer proximity of the methyl group to the histidine, potentially enhancing the binding affinity.[25] On the other hand, glycopeptide **4** was strategically designed as a negative control to impair the affinity towards antibody 5E5 by positioning the fluorine atom on the Pro residue towards the aromatic ring of Tyr100^L.

All glycopeptides were synthesized using microwave-assisted solid-phase peptide synthesis, following a protocol we previously reported (Supporting Information).[18b] The synthesis of the glycosyl amino acid building blocks for the preparation of compounds **2** and **8** has been previously reported by us.[18a,28] The synthetic route for the building block required for glycopeptide **3** is described in Scheme S1. Finally, compound **14** was synthesized according to our methodology with the modifications shown in Scheme S2.[29]

Binding Studies of Glycopeptides 1–9 with 5E5 and SM3 Monoclonal Antibodies
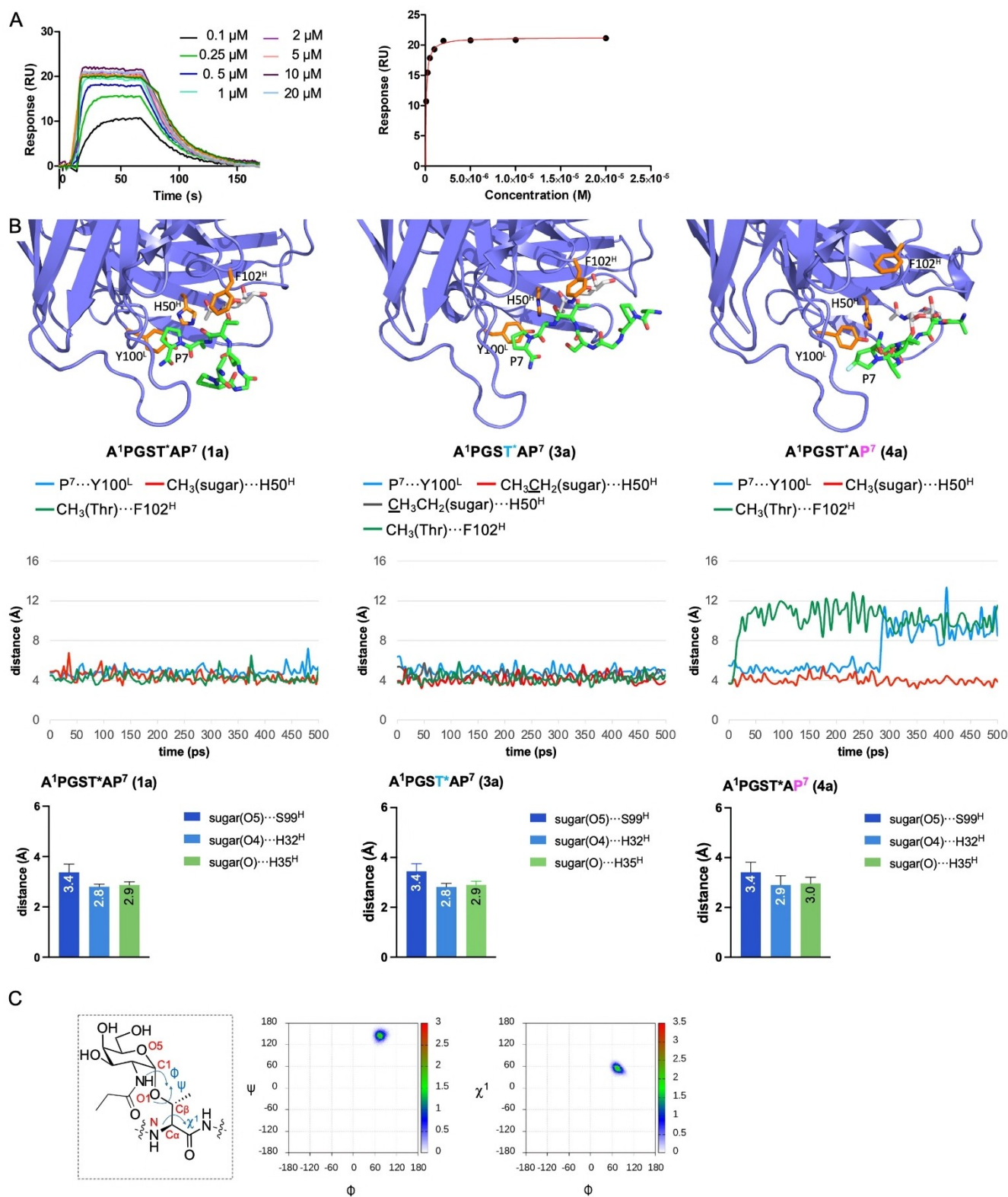
We used a standard surface plasmon resonance (SPR) assay to evaluate the binding affinity (K_D) of short peptides **1**–**9** to SM3 and 5E5 (Table 1 and Figures 3A and S1). These values represent the affinity of homogeneous monomeric antigens towards the immobilized antibody in a 1:1 binding model.[30] Remarkably, a significant increase in binding strength was observed in two cases compared to their natural counter-

Table 1: Binding affinities (K_D) of short peptides **1**–**9** to antibodies 5E5 and SM3 determined via an SPR assay.

Peptide	K_D (µM)[a]
5E5	
1	0.54 ± 0.10
2	0.64 ± 0.14
3	0.08 ± 0.01
4	2.40 ± 0.13
SM3	
5	0.89 ± 0.05
6	2.19 ± 0.21
7	1.62 ± 0.11
8	1.46 ± 0.18
9	0.13 ± 0.01

[a] Means ± standard deviation from 3 assays.

parts: glycopeptides **3** and **9** bound with 7-fold increased affinity to 5E5 and SM3, respectively. The comparable affinity of glycopeptide **8** and its natural counterpart **5** is consistent with the results in our previous study where we describe in detail the impact of Hnv in the PDT*R region on SM3 binding.[18a] In compounds **2** and **6**, replacing a C–H moiety with a C–F in the methyl group of GalNAc does not enhance the binding affinity. A plausible explanation is that the favorable polarizing influence exerted by the fluorine atom on the proposed CH/π contact, is counterbalanced by the concomitant decrease in the number of CH groups

Figure 3. (A) SPR curves (left panel) and the response−concentration fit (right panel) for glycopeptide **3** binding to antibody 5E5. (B) Representative frames derived from MD simulations for antibody scFv-5E5 in complex with the *truncated version* of glycopeptide **1** (**1a**, left panel), **3** (**3a**, middle panel) and **4** (**4a**, right panel); evolution of the distances between antibody residues Y100^L, H50^H and F102^H and the glycopeptides residues mainly involved in molecular recognition; to estimate the distances, the center of the aromatic rings was used in these calculations; hydrogen bond lengths between the sugar and the antibody. (C) Molecular structure showing the atoms involved in dihedral angle definition (left panel, $\phi = $ O5-C1-O1-Cβ; $\psi = $ C1-O1-Cβ-Cα; $\chi^1 = $ O1-Cβ-Cα-N). Plots of the ϕ/ψ and ϕ/χ^1 distributions derived from MD simulations of the complex **3a**/scFv-5E5 (right panels).

Angew. Chem. Int. Ed. **2024**, e202407131 (5 of 12)

© 2024 Wiley-VCH GmbH

available for interaction. Indeed, similar effects have been previously reported by Barbero and co-workers.[31] Additionally, changes in the solvophobic contribution promoted by the fluorine atom may also contribute to the lower affinity for their respective antibodies compared to their natural counterparts, compounds **1** and **5**.[31] In fact, the X-ray structure of an analog of glycopeptide **6** in complex with scFv-SM3 reveals the lack of CH/π interactions between the GalNAc and the aromatic side chain of Trp33^H.The distance between these groups is 8.4 Å, significantly greater than the 4.7 Å observed for a naturally occurring analog.[28]

To gain insight into the origin of the affinity of glycopeptides **1**, **3** and **4** for the 5E5 antibody, we performed molecular dynamics (MD) simulations with a truncated version of these glycopeptides (compounds **1a**, **3a** and **4a**, Figure 3B) in complex with scFv-5E5. We conducted three independent 500 ns MD simulations for each complex, resulting in a total trajectory time of 1.5 µs per complex (Figures 3B, 3 C and S3). In the case of glycopeptide **3a**, these calculations confirm that the N-propionyl group of the sugar and the C-terminal Pro residue interact through CH/π interactions with His50^H and Tyr100^L, respectively, analogously to what observed for the truncated version of the natural counterpart (referred to as **1a** in Figure 3B) in the X-ray structure reported by us.[25] These interactions are also observed in the simulations conducted in this work on the complex **1a**/scFv-5E5 (Figure 3B), validating our computational approach. Yet, the simulation shows an additional CH/π interaction between the CH$_3$CH$_2$ group of **3a** and the antibody, which is not present for **1a** suggesting that such a contact may improve the affinity of glycopeptide **3** compared to **1**. In contrast, glycopeptide **4**, which was designed as a negative control, shows a different behavior. The incorporation of a (4S)-4-fluoro-L-proline residue into glycopeptide **4** (modeled as **4a**, Figure 3B) does not modify the interactions between the sugar and the antibody. However, this substitution prevents the CH/π interaction P^7–Y100^L, and has a negative impact on the CH$_3$(Thr)–F102^H interaction as clearly shown by the distance evolution traces for the molecular moieties involved in these interactions. This result provides an explanation for the lower affinity observed for **4** in comparison to glycopeptides **1** and **3**.

Furthermore, according to our MD simulations (Figures 3C and S3), the glycosidic linkage is rather rigid for all the three peptides, displaying the exo-anomeric conformation centered at $\phi/\psi \approx 65°/120°$ in all replicas, which agrees with the typical eclipsed conformation found for the Tn-Thr derivatives.[32] Moreover, the side chain of the glycosylated residues is rigid in solution with a conformer characterized by $\chi^1 = 60°$.

In parallel we have conducted ITC assays with glycopeptides **1** and **3** (see Supporting Information and Figure S2). The ITC data indicate that the affinity of the unnatural glycopeptide **3** is 5-fold higher than that of the natural glycopeptide (compound **1**), which agrees well with the SPR data, showing approximately a 7-fold enhancement. In both cases, the binding is driven by enthalpy ($\triangle H_{\textbf{1-Ac}} = -8.19$ kcal/mol and $\triangle H_{\textbf{3-Ac}} = -9.15$ kcal/mol), with a difference of about 1 kcal/mol in favor of the unnatural glycopeptide. This result

is consistent with our MD simulations, which suggest an enhancement of the CH/π interaction in glycopeptide **3**.

Validation of the Designed Glycopeptides as TA-MUC1 Model Antigens: Development of a Dot-Blot Assay

Gold nanoparticles (AuNPs) have been successfully used in diagnostic immunoassays, mostly in the form of lateral flow assays.[33] Most commonly, AuNP-based immunoassays exploit antibody-functionalized nanoparticles. However, it is also possible to immobilize antigens on AuNPs and to develop serological (antibody) tests.[34] We have previously reported on the preparation of AuNPs functionalized with TA-MUC1 glycopeptides as immunogenic formulations.[18a,b,35] These nanoparticles present multiple copies of the peptide immobilized on top of a compact, self-assembled monolayers of amphiphilic alkyl-PEG600 thiols[36] anchored to the gold surface. Similar coatings were shown to allow unhindered protein-receptor interaction,[37] and unhindered enzymatic cleavage of DNA – RNA heteroduplexes,[38] most likely due to their hydrophilic nature.[39]

We envisioned the possibility of using analogous nanoparticles for the development of a serological assay, although with a reduced antigen loading to favor unhindered antigen-antibody interaction. Briefly, AuNPs with a 13 nm core diameter were surface coated (passivated) with a mixture of carboxy- and amino-terminated alkyl-PEG600 thiols. Then, thiolated antigen models (glycopeptides **1'–13'** Supporting Information, or compound **14**) were coupled to the nanoparticle coating using an amine-to-thiol heterobifunctional linker (Figure S4). As previously demonstrated, peptide loading can be controlled by varying the molar fraction of amino terminated PEG600 derivative x_{NH2} during the passivation reaction.[36] In this study, we used $x_{NH2} = 0.06$ which resulted in a peptide loading of approximately 50 peptides/AuNP as estimated by amino acid analysis.[37] Successful glycopeptide conjugation was confirmed via agarose gel electrophoresis (Figure S5). All prepared AuNPs (**AuNP1–14**) are negatively charged as indicated by their electrophoretic migration towards the cathode and confirmed by the negative ζ-potential (Table S1). In case of **AuNP14** that are functionalized with Tn mimic **14** – a small neutral molecule – only minor differences in physicochemical properties were observed when compared to the passivated nanoparticles used as a starting material (**AuNP-PEG**, Figure S4). Nevertheless, an evident and reproducible electrophoretic shift was observed (Figure S5), demonstrating nanoparticle functionalization. Further evidence for the conjugation of compound **14** was provided by a lectin-driven aggregation assay (Figures S6 and S7).[40] Both **AuNP14** and **AuNP11** (with a Tn antigen in the PDT*R region, used as a positive control) underwent aggregation upon titration with soybean agglutinin (SBA), a well-established, commercially available lectin with selectivity for GalNAc in the context of O-linked glycopeptides.[41] These results confirmed that nanoparticles **AuNP14** were indeed functionalized with glycan-like structures that mimic Tn.
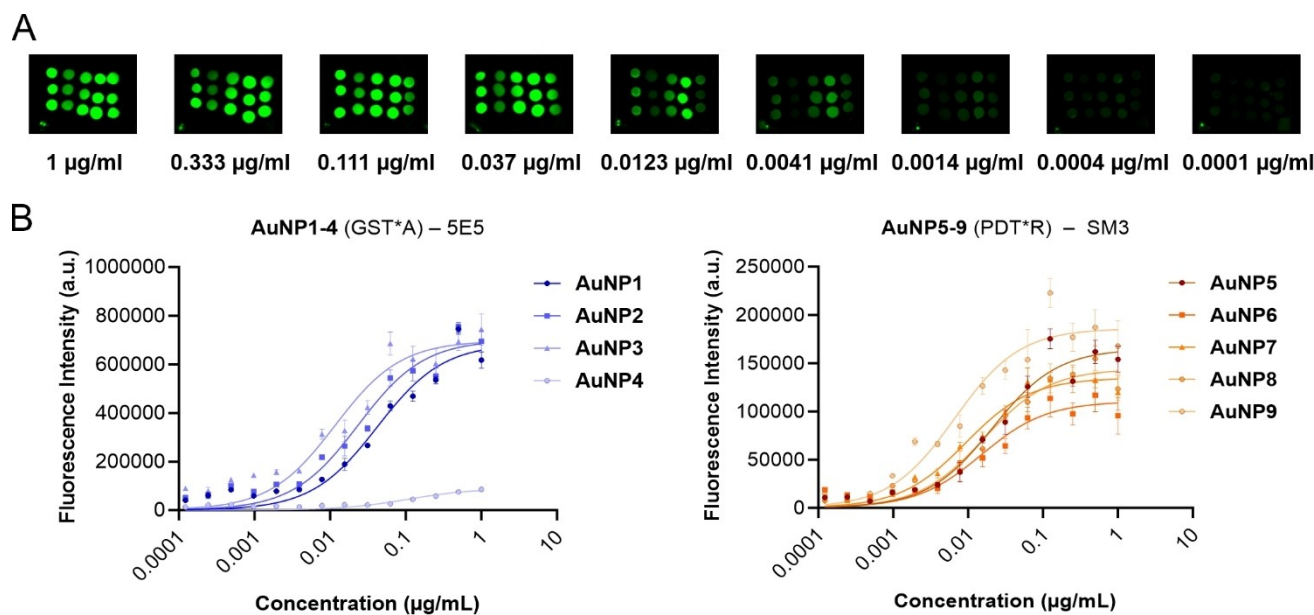
Figure 4. (A) Representative fluorescence images of the membranes used for the determination of the binding affinity of 5E5 antibody to **AuNP1–4** and **AuNP12** via a dot-blot assay. Each column of dots corresponds to a different AuNP probe with three technical replicates. Images are shown in false colors. (B) Binding curves for monoclonal antibodies 5E5 or SM3 to AuNP probes **AuNP1–9** displaying TA-MUC1 model antigens. The K_{Dapp} values were obtained via a nonlinear curve fitting – using a one-site binding equation – of the fluorescence intensity values (average of the 3 technical replicates) measured at varying antibody concentration. The K_{Dapp} values are reported in Tables 2 and 3.

Next, we developed a dot-blot assay to investigate the binding of monoclonal antibodies SM3 and 5E5 to nanoparticles **AuNP1–14**. These experiments were required to validate antibody binding in the context of the diagnostic assay format that we later applied to the human serum specimens. Differently from the SPR measurements reported above, in this case the antigens are immobilized (on the AuNP surface) while the antibodies are free in solution. Multivalent antigen presentation on a surface allows for bivalent antibody binding which is essentially irreversible as observed in many cases.[42] This implicates that binding affinities cannot be measured under equilibrium conditions. Therefore, the results of these experiments (K_{Dapp}, apparent binding affinities from a one site - specific binding model) should be taken as association or affinity parameters[43] and not as thermodynamic constants and used only for comparison purposes among the different library members under the specified experimental conditions. To this purpose, the functionalized AuNPs were spotted onto nitrocellulose membranes and adsorbed by physisorption. After spotting, the membranes were subjected to a series of washing and blocking steps before overnight incubation at 4°C with antibodies SM3 or 5E5 (see details in the Supporting Information). The membranes were then washed again and incubated with a fluorescently labeled anti-mouse secondary antibody. The final step was the visualization of the membranes with a laser scanner. The acquired images were quantitatively analyzed by densitometry. This approach allowed the evaluation of the binding affinity of each antibody for 5 to 7 nanoparticle probes in parallel. In fact, the selected nanoparticle probes were applied to separate membranes and each membrane was incubated independ-

ently and in parallel with different concentrations of a particular antibody. Then for each nanoparticle probe, a plot of integrated fluorescence intensity versus antibody concentration was generated (Figure 4). The data were fitted to a one-site binding model, affording an apparent binding affinity designated K_{Dapp}.[43] These values are a measure of the affinity of the selected antibody for a given antigen on a multivalent scaffold – specifically nanoparticles **AuNP1–14**.[44]

We initially evaluated and compared the binding of 5E5 and SM3 to nanoparticles functionalized with full-length tandem repeat peptides to validate the dot-blot assay. From the data in Table 2, it is possible to appreciate that 5E5 binds as expected to **AuNP10** and **AuNP12**, both displaying natural glycopeptides containing the GST*A region.[45]

It is also worth noting that the K_{Dapp} values measured in this work are lower compared to a previously reported value for a not immobilized GST*A peptide (1.7 nM,)[46] likely as

Table 2: Apparent binding affinities of SM3 and 5E5 antibodies for full-length tandem repeat MUC1 glycopeptides immobilized on AuNPs.[a]

| Probe | K_{Dapp}/µg/mL (nM)[a] | |
	SM3	5E5
AuNP10	>2	0.023 ± 0.010 (0.15)
AuNP11	0.023 ± 0.016 (0.15)	>10
AuNP12	0.029 ± 0.005[b] (0.19)	0.027 ± 0.004 (0.18)
AuNP13	0.038 ± 0.006 (0.25)	>10

[a] Means ± standard deviation from 3–6 assays; values within brackets are expressed in nM assuming 150 kDa as the molar mass of the antibodies. [b] Mean value ± 0.5×max. deviation from 2 assays.

a result of divalent antibody binding to the multivalent AuNP probes. Also, consistent with the known selectivity of 5E5, no binding was observed for **AuNP11** or for the unnatural version **AuNP13**, which lacks the GalNAc unit in the GSTA region required for binding.[25,45] The results with SM3 were also consistent with its known binding characteristics. SM3 bound to **AuNP11–13**, all displaying the PDT*R region,[18f] whether in its natural form or as an unnatural mimic. A much weaker binding was instead observed for **AuNP10**, which displays the unglycosylated PDTR sequence.[45] These results are in line with those previously reported by us for full-length tandem repeat glycopeptides **11** and **13** using biolayer interferometry experiments.[18a]

Overall, these results validate the binding assay, which was then used to screen the affinity of the two selected antibodies for all other nanoparticles in the library (Table 3). **AuNP1–9** display sequences with only nine amino acids including one single binding motif specific for either 5E5 or SM3. According to their sequences, **AuNP1–4** were assayed with 5E5 and **AuNP5–9** with SM3, respectively. Each of these two groups contained nanoparticles with the natural version of the peptide (**AuNP1** and **AuNP5**) as a reference. In all cases, except for **AuNP4** used as a negative control, binding was retained, albeit with small variations compared to the natural peptides. These results are in close agreement with the results of the SPR analysis of the free glycopeptides, except for derivative **AuNP6**, which shows comparable binding to the other nanoparticle probes of the SM3 series, although free peptide **6** had detectably lower affinity in the SPR assay. This discrepancy is most likely a consequence of the different approaches for estimating antigen-antibody affinity whereby binding of antibodies to immobilized antigens is implicitly affected by the bivalent nature of the antibody. Finally, **AuNP14**, displaying the Tn mimic, was assayed both against SM3 and 5E5 because the presented antigen model lacks a peptide backbone. No binding was observed to any of the two antibodies consistently with the notion that these antibodies not only recognize the sugar moiety but also the peptide sequence.[18f,25]

Table 3: Apparent binding affinities of antibodies 5E5 and SM3 for short TA-MUC1 antigen models immobilized on AuNPs.

Probe	K_{Dapp} (µg/mL)[a]
5E5	
AuNP1	0.025 ± 0.012
AuNP2	0.018 ± 0.005
AuNP3	0.010 ± 0.002
AuNP4	> 2
SM3	
AuNP5	0.017 ± 0.004
AuNP6	0.019 ± 0.003
AuNP7	0.011 ± 0.002
AuNP8	0.017 ± 0.001[b]
AuNP9	0.0066 ± 0.0004

[a] Means $\pm$ standard deviation from 3–6 assays. [b] Mean value $\pm$ 0.5$\times$max. deviation from 2 assays.

These studies show that the conjugation of the model antigens to the surface of the nanoparticles does not have a major impact on the antigen-antibody interaction. Additionally, our library allowed us to directly compare the effect of shortening the probing peptide sequences on the nanoparticles, which turned out to be very limited (**AuNP1** vs. **AuNP10** and **AuNP5** vs. **AuNP11**).

Detection of TA-MUC1 Autoantibodies in Sera

After having established the dot-blot assay, we applied it to the detection of autoantibodies against TA-MUC1 in sera specimens. To this purpose, we designed a retrospective, observational, case-control clinical study recruiting a group of 20 pancreatic cancer patients and 20 age- and sex-matched healthy volunteers at the Hospital San Pedro (Logroño, Spain).

The serum samples were analyzed against the complete nanoparticle library. Each nanoparticle probe, corresponding to a distinct TA-MUC1 antigen model, was spotted in triplicate on wet nitrocellulose membranes (Figure S8). For each patient (or healthy volunteer) the serum was analyzed in triplicate, i.e. on three individual membranes. The binding of IgG autoantibodies to the spotted AuNP probes was revealed by incubation with a fluorescently labelled DyLight™ 800 anti-human IgG secondary antibody. Data normalization and exhaustive statistical analysis are detailed in the Supporting Information.

The resulting normalized fluorescence intensities for pancreatic cancer patients (cases, red) and healthy volunteers (controls, blue) are shown in Figure 5A and the corresponding p-values are reported in Table S2. These results are obtained with the limitation of having normalized cases and controls separately. Therefore, data analysis was further refined carrying out a permutation test. In simple words, the null hypothesis of this test states that, for each AuNP probe, all fluorescence intensities come from the same distribution and therefore cases and controls cannot be distinguished. The result of this test (Table S3) confirmed the null-hypothesis for all nanoparticle probes displaying (un)natural glycopeptides mimicking the PDT*R epitope (**AuNP5–9**, **AuNP11**, and **AuNP13**, labels in red in X-axis of Figure 5A) which therefore cannot not be used to stratify cases vs. controls. Notably, **AuNP14** probe gave substantially higher fluorescence intensities for both cases and controls but also did not allow discrimination. This last result indicates that the Tn mimic on **AuNP14** is recognized by autoantibodies that are present in all individuals, likely Tn autoantibodies,[47] but their presence cannot be used for diagnostic purposes because it is not specific for cancer.

Remarkably, AuNP probes displaying (un)natural glycopeptides mimicking the GST*A epitope with GalNAc glycosylation, i.e. the 5E5 epitope, can instead discriminate between cases and controls (**AuNP1–3**, **AuNP10**, and **AuNP12**, labels in black on the X-axis of Figure 5A). **AuNP4**, presenting a glycopeptide with a weak affinity to 5E5 that was used as a negative control, is the only nanoparticles of this group not able to discriminate cases vs.
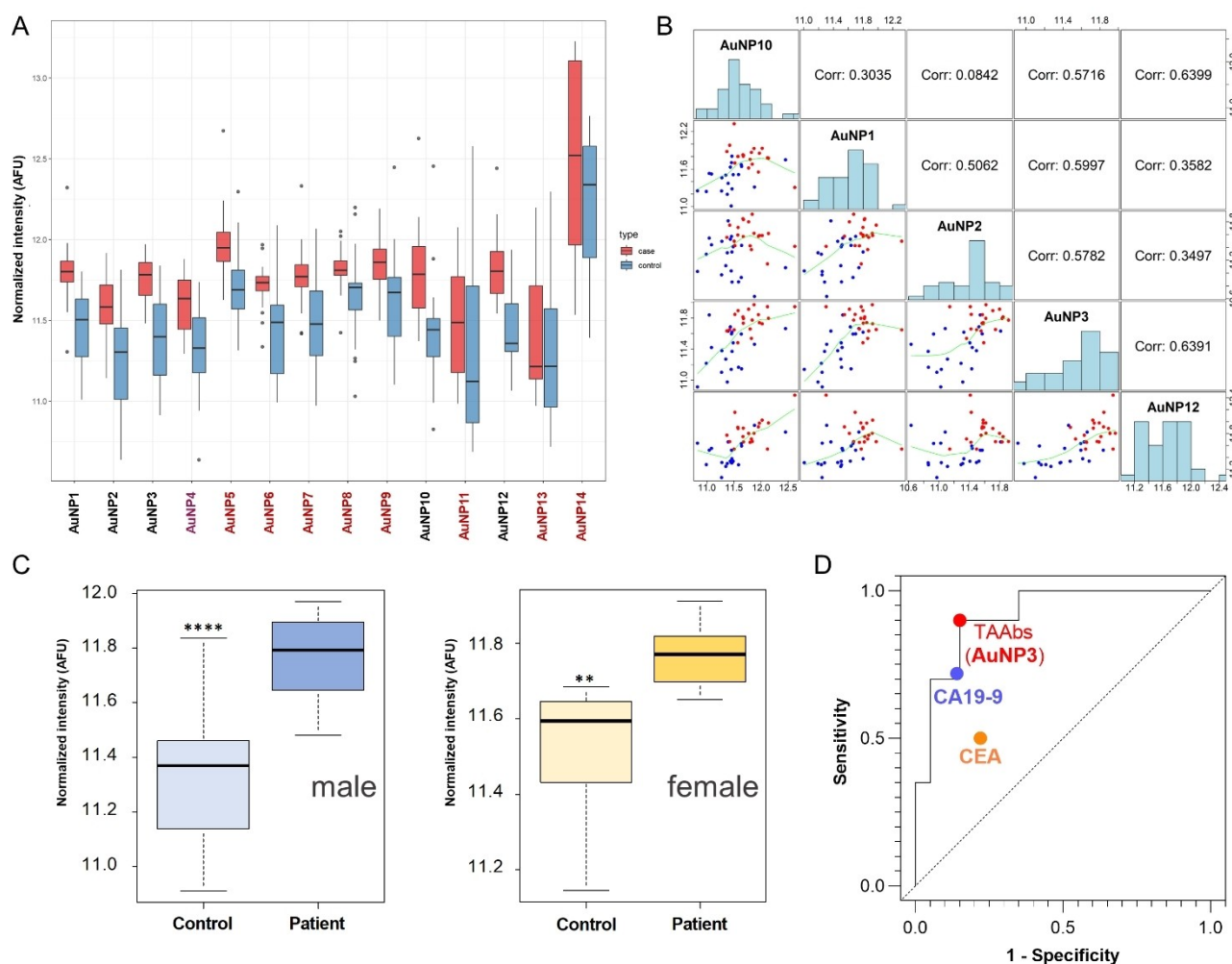
Figure 5. Results of the serological assay using AuNP probes to detect TA-MUC1 autoantibodies in the sera of pancreatic cancer patients and healthy volunteers. (A) Normalized fluorescence intensities for PC cases in red and healthy controls in blue. Labels in red on the X-axis indicate probes that do not discriminate cases and controls after application of a permutation test. Labels in black are for probes with diagnostic potential. (B) Scatter plot matrix showing histograms and correlations between the integrated intensity data obtained for patients (red dots) and controls (blue dots) for AuNP probes that discriminate cases and controls. (C) Antibody levels in healthy volunteers (control) and in pancreatic cancer patients divided by sex using **AuNP3**. Box plots represent the interquartile range with the median as a horizontal line. Whiskers encompass the maximum and minimum values of the population. **: $p < 0.01$; ****: $p < 0.0001$. (D) Receiver operating characteristic (ROC) curve for TA-MUC1 autoantibodies detected by **AuNP3**. The area under the curve (AUC) is 0.918 (95% confidence interval: 0.832–1.000), 85% sensitivity, 90% specificity (red dot) with a threshold at 11.63 arbitrary fluorescence units (AFU). Blue dot (CA19-9) and orange dot (CEA) are also plotted for comparison using sensitivity and specificity values from recent meta-analysis studies.[5,50]

controls. This result is in agreement with the knowledge that the Tn-GSTA epitope is highly cancer-specifically expressed as shown by 5E5 immunohistochemistry and that only Tn-GSTA induces IgG antibodies after vaccination in cancer/older people.[27] Additionally, antibody 5E5 has been used to produce chimeric antigen receptor T cells (CAR-T cells) that effectively suppressed tumor growth in pancreatic cancer.[48]

Next, a correlation analysis was performed to identify redundant data. For probes **AuNP1–3**, **AuNP10**, and **AuNP12**, affording fluorescence signals that show association with disease status, moderate-to high correlation can be observed for every probe pair (Figures 5B and S9). This result is not unexpected since the displayed model antigens

on each AuNP probe are "small" variations of the same structural theme, namely the GST*A epitope. It also suggests that stratification of pancreatic cancer patients vs. healthy volunteers can be possibly achieved using just one single AuNP probe. Correlation coefficients > 0.57 were observed between the data obtained with **AuNP3** and data from the other discriminating AuNP probes (**AuNP1**, **2**, **10** and **AuNP12**), suggesting that serum analysis with this probe encompasses most of the information obtainable with any of the other probes. The data obtained with **AuNP1** are however only modestly correlated with those obtained with **AuNP10** and **AuNP12**, which display full-length tandem repeat sequences with the natural Tn antigen. This modest correlation implies that **AuNP1** binds a somewhat different

subset of autoantibodies compared to the AuNP probes with full-length natural peptides, possibly because it displays only a single epitope mimic. Therefore, our data analysis further focused on data obtained with **AuNP3**, which combines structural simplicity with very good association properties.

The normalized fluorescence intensity data from the sera analysis with **AuNP3** were statistically tested against sex and age variables (Figure 5C). There was no correlation with either sex ($p=0.37$) or age ($p=0.40$) indicating indistinguishable MUC1 autoantibodies levels in groups based on these variables. Furthermore, sex specific case/control analysis shows that patient stratification is not sex sensitive. The relationship between MUC1 autoantibodies levels and various other clinical parameters was also examined (Table S4). No significant correlations were identified. Interestingly, there was also no correlation with other biomarkers currently in use for the follow-up of pancreatic cancer, such as CA19-9 and carcinoembryonic antigen (CEA), *suggesting that autoantibodies against MUC1 are an independent biomarker and could improve the diagnosis of pancreatic cancer beyond current possibilities.*

Finally, to better understand the biomarker potential of the autoantibodies identified by probe **AuNP3**, a receiver operating characteristic (ROC) curve[49] was built (Figure 5D). The curve illustrates the relationship between sensitivity, which represents the fraction of actual positives correctly assigned by the test, and specificity, denoting the fraction of actual negatives. For probe **AuNP3**, an area under the curve (AUC) of 0.918 was obtained, with a sensitivity of 85 % and specificity of 90 %.

In comparison, in recent meta-analysis studies, the AUC for the antigen CA19-9 was 0.8474 (sensitivity 72 % and specificity 86 %),[5] while for the carcinoembryonic antigen (CEA) was 0.67 (sensitivity 50 % and specificity 78 %).[50] These values demonstrate that the tumor associates autoantibodies detected by **AuNP3** outperform CA19-9 and CEA antigens in terms of both sensitivity and specificity, establishing them as a promising biomarker for pancreatic cancer detection.

Conclusions

Here we present a dot-blot-based assay for the detection of circulating tumor-associated autoantibodies against MUC1 with diagnostic potential for pancreatic cancer (PC). To this end, we combined X-ray information and molecular modeling to design a library of (un)natural glycopeptides binding to two monoclonal antibodies – SM3 and 5E5 – that have been developed to recognize TA-MUC1 and are characterized by distinct epitopes both affected by glycosylation. We validated the design of our model antigens by SPR analysis and used them to prepare a library of nanoparticle probes. These probes were used in a dot blot assay for antibody detection, which was validated against SM3 and 5E5. Finally, the library of nanoparticle probes was used to detect TA-MUC1 IgG autoantibodies in sera from PC patients and healthy volunteers. Our results show that nanoparticle probes that were good binders of 5E5 (i.e. with glycopep-

tides mimicking the GST*A epitope) discriminated between PC cases and controls. In contrast, none of the nanoparticle probes that were good binders of SM3 (i.e. with glycopeptides mimicking the PDT*R epitope) achieved this goal.

Autoantibodies to MUC1 and aberrant glycoforms of MUC1 have been widely detected in cancer patients, but studies so far have not been able to establish their diagnostic value.[16b] One reason could be the use of assays involving larger MUC1 antigens with multiple epitopes (i.e. PDTR and GSTA +/-Tn etc.) while here we dissect the MUC1 epitome down to single, distinct, epitope mimic and present them on individual multivalent probes. Remarkably **AuNP3**, one of the nanoparticle probes with highest discriminatory potential, displays a short glycopeptide with an unnatural modification on the saccharide residue suggesting that our structural based approach may help selecting autoantibodies subsets that have higher tumor specificity. The autoantibodies detected by this probe show significantly better true and false positive rates for PC identification than current clinical biomarkers and are suggested as an independent biomarker that could improve disease diagnosis.

Finally, we also emphasize that our approach has allowed the development of TA-MUC1 model antigens that are short and simple glycopeptides significantly reducing the synthetic effort and increasing their attractivity for clinical diagnostic applications. Future work is focused on the development of more selective glycopeptide nanoparticle probes and on the application of our diagnostic assay in suitable validation cohorts.

Supporting Information

Synthesis and characterization of glycopeptides and Tn mimic **14**, SPR curves, MD simulations, preparation and characterization of the nanoparticle probes, lectin binding assay, clinical sample collection, dot-blot assays on serum samples, data analysis and statistical analysis of the dot-blot assay results.

Acknowledgements

Conflict of Interest

The authors declare the following competing financial interest: A.A., A.E, M.P.M.-M., E.d.T., G.M., R.F., A.M., and F.C. are co-inventors on a patent application (ref. PCT/ES2024/070001, filed on 19th January 2023) that protects methods for detection of pancreatic cancer, as described in this study.

Data Availability Statement

The data that support the findings of this study are available from the corresponding author upon reasonable request.

[1] H. Sung, J. Ferlay, R. L. Siegel, M. Laversanne, I. Soerjomataram, A. Jemal, F. Bray, *Ca-Cancer J. Clin.* **2021**, *71*, 209–249.

[2] a) K. Dumstrei, H. Chen, H. Brenner, *Oncotarget* **2016**, *7*, 11151–11164; b) J. Yang, R. Xu, C. Wang, J. Qiu, B. Ren, L. You, *Cancer Commun.* **2021**, *41*, 1257–1274.

[3] R. L. Siegel, K. D. Miller, H. E. Fuchs, A. Jemal, *Ca-Cancer J. Clin.* **2022**, *72*, 7–33.

[4] G. Luo, K. Jin, S. Deng, H. Cheng, Z. Fan, Y. Gong, Y. Qian, Q. Huang, Q. Ni, C. Liu, X. Yu, *Biochim. Biophys. Acta* **2021**, *1875*, 188409.

[5] B. Zhao, B. Zhao, F. Chen, *Eur. J. Gastroenterol. Hepatol.* **2022**, *34*, 891–904.

[6] M. A. Tempero, M. P. Malafa, M. Al-Hawary, H. Asbun, A. Bain, S. W. Behrman, A. B. Benson, E. Binder, D. B. Cardin, C. Cha, E. G. Chiorean, V. Chung, B. Czito, M. Dillhoff, E. Dotan, C. R. Ferrone, J. Hardacre, W. G. Hawkins, J. Herman, A. H. Ko, S. Komanduri, A. Koong, N. LoConte, A. M. Lowy, C. Moravek, E. K. Nakakura, E. M. O'Reilly, J. Obando, S. Reddy, C. Scaife, S. Thayer, C. D. Weekes, R. A. Wolff, B. M. Wolpin, J. Burns, S. Darlow, *J. Natl. Compr. Cancer Network* **2017**, *15*, 1028–1061.

[7] L. Zhuang, C. Huang, Z. Ning, L. Yang, W. Zou, P. Wang, C.-S. Cheng, Z. Meng, *Int. J. Cancer* **2023**, *152*, 1013–1024.

[8] a) H. T. Tan, J. Low, S. G. Lim, M. C. M. Chung, *FEBS J.* **2009**, *276*, 6880–6904; b) C. Desmetz, A. Mange, T. Maudelonde, J. Solassol, *J. Cell. Mol. Med.* **2011**, *15*, 2013–2024.

[9] J. Wu, X. Li, W. Song, Y. Fang, L. Yu, S. Liu, L. P. Churilov, F. Zhang, *Autoimmun. Rev.* **2017**, *16*, 1270–1281.

[10] U. Karsten, S. von Mensdorff-Pouilly, S. Goletz, *Tumor Biol.* **2005**, *26*, 217–220.

[11] a) J. Taylor-Papadimitriou, J. M. Burchell, R. Graham, R. Beatson, *Biochem. Soc. Trans.* **2018**, *46*, 659–668; b) V. Apostolopoulos, L. Stojanovska, S. E. Gargosky, *Cell. Mol. Life Sci.* **2015**, 1–26.

[12] N. Remmers, J. M. Anderson, E. M. Linde, D. J. DiMaio, A. J. Lazenby, H. H. Wandall, U. Mandel, H. Clausen, F. Yu, M. A. Hollingsworth, *Clin. Cancer Res.* **2013**, *19*, 1981.

[13] a) S. S. Pinho, C. A. Reis, *Nat. Rev. Cancer* **2015**, *15*, 540–555; b) S. Nath, P. Mukherjee, *Trends Mol. Med.* **2014**, *20*, 332–342; c) D. W. Kufe, *Nat. Rev. Cancer* **2009**, *9*, 874–885.

[14] a) M. V. Croce, M. T. Isla-Larrain, S. O. Demichelis, A. Segal-Eiras, J. R. Gori, M. R. Price, *Breast Cancer Res. Treat.* **2003**, *81*, 195–207; b) J. P. Pandey, A. M. Namboodiri, E. Kistner-Griffin, *Hum. Immunol.* **2013**, *74*, 1030–1033.

[15] Y. Tang, L. Wang, P. Zhang, H. Wei, R. Gao, X. Liu, Y. Yu, L. Wang, *Clin. Vaccine Immunol.* **2010**, *17*, 1903.

[16] a) O. Blixt, D. Bueti, B. Burford, D. Allen, S. Julien, M. Hollingsworth, A. Gammerman, I. Fentiman, J. Taylor-Papadimitriou, J. M. Burchell, *Breast Cancer Res.* **2011**, *13*, R25; b) B. Burford, A. Gentry-Maharaj, R. Graham, D. Allen, J. W. Pedersen, A. S. Nudelman, O. Blixt, E. O. Fourkala, D. Bueti, A. Dawnay, J. Ford, R. Desai, L. David, P. Trinder, B. Acres, T. Schwientek, A. Gammerman, C. A. Reis, L. Silva, H. Osório, R. Hallett, H. H. Wandall, U. Mandel, M. A. Hollingsworth, I. Jacobs, I. Fentiman, H. Clausen, J. Taylor-Papadimitriou, U. Menon, J. M. Burchell, *Br. J. Cancer* **2013**, *108*, 2045–2055; c) H. H. Wandall, O. Blixt, M. A. Tarp, J. W. Pedersen, E. P. Bennett, U. Mandel, G. Ragupathi, P. O. Livingston, M. A. Hollingsworth, J. Taylor-Papadimitriou, J. Burchell, H. Clausen, *Cancer Res.* **2010**, *70*, 1306.

[17] a) O. J. Finn, *Cancer Immunol. Res.* **2017**, *5*, 347–354; b) C. Jacqueline, O. J. Finn, *Semin. Immunol.* **2020**, *47*, 101394.

[18] a) I. A. Bermejo, A. Guerreiro, A. Eguskiza, N. Martínez-Sáez, F. S. Lazaris, A. Asín, V. J. Somovilla, I. Compañón, T. K. Raju, S. Tadic, P. Garrido, J. García-Sanmartín, V. Mangini, A. S. Grosso, F. Marcelo, A. Avenoza, J. H. Busto, F. García-Martín, R. Hurtado-Guerrero, J. M. Peregrina, G. J. L. Bernardes, A. Martínez, R. Fiammengo, F. Corzana, *JACS Au* **2024**, *4*, 150–163; b) I. Compañón, A. Guerreiro, V. Mangini, J. Castro-López, M. Escudero-Casao, A. Avenoza, J. H. Busto, S. Castillón, J. Jiménez-Barbero, J. L. Asensio, G. Jiménez-Osés, O. Boutureira, J. M. Peregrina, R. Hurtado-Guerrero, R. Fiammengo, G. J. L. Bernardes, F. Corzana, *J. Am. Chem. Soc.* **2019**, *141*, 4063–4072; c) V. J. Somovilla, I. A. Bermejo, I. S. Albuquerque, N. Martínez-Sáez, J. Castro-López, F. García-Martín, I. Compañón, H. Hinou, S.-I. Nishimura, J. Jiménez-Barbero, J. L. Asensio, A. Avenoza, J. H. Busto, R. Hurtado-Guerrero, J. M. Peregrina, G. J. L. Bernardes, F. Corzana, *J. Am. Chem. Soc.* **2017**, *139*, 18255–18261; d) V. Rojas-Ocáriz, I. Compañón, C. Aydillo, J. Castro-Loŕez, J. Jiménez-Barbero, R. Hurtado-Guerrero, A. Avenoza, M. M. Zurbano, J. M. Peregrina, J. H. Busto, F. Corzana, *J. Org. Chem.* **2016**, *81*, 5929–5941; e) E. M. S. Fernández, C. D. Navo, N. Martínez-Sáez, R. Gonçalves-Pereira, V. J. Somovilla, A. Avenoza, J. H. Busto, G. J. L. Bernardes, G. Jiménez-Osés, F. Corzana, J. M. G. Fernández, C. O. Mellet, J. M. Peregrina, *Org. Lett.* **2016**, *18*, 3890–3893; f) N. Martínez-Sáez, J. Castro-Lõpez, J. Valero-González, D. Madariaga, I. Compañõn, V. J. Somovilla, M. Salvadõ, J. L. Asensio, J. Jiménez-Barbero, A. Avenoza, J. H. Busto, G. J. L. Bernardes, J. M. Peregrina, R. Hurtado-Guerrero, F. Corzana, *Angew. Chem. Int. Ed.* **2015**, *54*, 9830–9834.

[19] a) I. A. Bermejo, C. D. Navo, J. Castro-López, A. Guerreiro, E. Jiménez-Moreno, E. M. Sánchez Fernández, F. García-Martín, H. Hinou, S.-I. Nishimura, J. M. García Fernández, C. O. Mellet, A. Avenoza, J. H. Busto, G. J. L. Bernardes, R. Hurtado-Guerrero, J. M. Peregrina, F. Corzana, *Chem. Sci.*

2020, *11*, 3996–4006; b) N. Martinez-Saez, N. T. Supekar, M. A. Wolfert, I. A. Bermejo, R. Hurtado-Guerrero, J. L. Asensio, J. Jimenez-Barbero, J. H. Busto, A. Avenoza, G.-J. Boons, J. M. Peregrina, F. Corzana, *Chem. Sci.* **2016**, *7*, 2294–2301.

[20] P. A. Guillen-Poza, E. M. Sánchez-Fernández, G. Artigas, J. M. García Fernández, H. Hinou, C. Ortiz Mellet, S. I. Nishimura, F. Garcia-Martin, *J. Med. Chem.* **2020**, *63*, 8524–8533.

[21] M. A. Tarp, A. L. Sørensen, U. Mandel, H. Paulsen, J. Burchell, J. Taylor-Papadimitriou, H. Clausen, *Glycobiology* **2007**, *17*, 197–209.

[22] P. Dokurno, P. A. Bates, H. A. Band, L. M. D. Stewart, J. M. Lally, J. M. Burchell, J. Taylor-Papadimitriou, D. Snary, M. J. E. Sternberg, P. S. Freemont, *J. Mol. Biol.* **1998**, *284*, 713–728.

[23] B. Richichi, B. Thomas, M. Fiore, R. Bosco, H. Qureshi, C. Nativi, O. Renaudet, L. BenMohamed, *Angew. Chem. Int. Ed.* **2014**, *53*, 11917–11920.

[24] A. Amedei, F. Asadzadeh, F. Papi, M. G. Vannucchi, V. Ferrucci, I. A. Bermejo, M. Fragai, C. V. De Almeida, L. Cerofolini, S. Giuntini, M. Bombaci, E. Pesce, E. Niccolai, F. Natali, E. Guarini, F. Gabel, C. Traini, S. Catarinicchia, F. Ricci, L. Orzalesi, F. Berti, F. Corzana, M. Zollo, R. Grifantini, C. Nativi, *iScience* **2020**, *23*, 101250.

[25] J. Macías-León, I. A. Bermejo, A. Asín, A. García-García, I. Compañón, E. Jiménez-Moreno, H. Coelho, V. Mangini, I. S. Albuquerque, F. Marcelo, J. L. Asensio, G. J. L. Bernardes, H. J. Joshi, R. Fiammengo, O. Blixt, R. Hurtado-Guerrero, F. Corzana, *Chem. Commun.* **2020**, *56*, 15137–15140.

[26] P. V. Beum, J. Singh, M. Burdick, M. A. Hollingsworth, P.-W. Cheng, *J. Biol. Chem.* **1999**, *274*, 24641–24648.

[27] P. J. Sabbatini, G. Ragupathi, C. Hood, C. A. Aghajanian, M. Juretzka, A. Iasonos, M. L. Hensley, M. K. Spassova, O. Ouerfelli, D. R. Spriggs, W. P. Tew, J. Konner, H. Clausen, N. Abu Rustum, S. J. Dansihefsky, P. O. Livingston, *Clin. Cancer Res.* **2007**, *13*, 4170–4177.

[28] I. A. Bermejo, I. Usabiaga, I. Compañón, J. Castro-López, A. Insausti, A. Fernández, A. Avenoza, J. H. Busto, J. Jiménez-Barbero, J. L. Asensio, J. M. Peregrina, G. Jiménez-Osés, R. Hurtado-Guerrero, E. J. Cocinero, F. Corzana, *J. Am. Chem. Soc.* **2018**, *140*, 9952–9960.

[29] a) R. Gracia, M. Marradi, G. Salerno, R. Pérez-Nicado, A. Pérez-San Vicente, D. Dupin, J. Rodriguez, I. Loinaz, F. Chiodo, C. Nativi, *ACS Macro Lett.* **2018**, *7*, 196–200; b) J. Jiménez-Barbero, E. Dragoni, C. Venturi, F. Nannucci, A. Ardá, M. Fontanella, S. André, F. J. Cañada, H.-J. Gabius, C. Nativi, *Chem. Eur. J.* **2009**, *15*, 10423–10431.

[30] S. Hearty, P. Leonard, R. O'Kennedy, in *Antibody Engineering: Methods and Protocols, Second Edition* (Ed.: P. Chames), Humana Press, Totowa, NJ, **2012**, pp. 411–442.

[31] a) J. L. Asensio, A. Ardá, F. J. Cañada, J. Jiménez-Barbero, *Acc. Chem. Res.* **2013**, *46*, 946–954; b) L. Unione, M. Alcalá, B. Echeverria, S. Serna, A. Ardá, A. Franconetti, F. J. Cañada, T. Diercks, N. Reichardt, J. Jiménez-Barbero, *Chem. Eur. J.* **2017**, *23*, 3957–3965.

[32] F. Corzana, J. H. Busto, G. Jiménez-Osés, M. García de Luis, J. L. Asensio, J. Jiménez-Barbero, J. M. Peregrina, A. Avenoza, *J. Am. Chem. Soc.* **2007**, *129*, 9458–9467.

[33] a) D. Lou, L. Fan, T. Jiang, Y. Zhang, *VIEW* **2022**, *3*, 20200125; b) R. Banerjee, A. Jaiswal, *Analyst* **2018**, *143*, 1970–1996.

[34] a) T. T. S. Lew, K. M. M. Aung, S. Y. Ow, S. N. Amrun, L. Sutarlie, L. F. P. Ng, X. Su, *ACS Nano* **2021**, *15*, 12286–12297; b) H. Andresen, M. Mager, M. Grießner, P. Charchar, N. Todorova, N. Bell, G. Theocharidis, S. Bertazzo, I. Yarovsky, M. M. Stevens, *Chem. Mater.* **2014**, *26*, 4696–4704; c) R. Salem, A. M. Elshamy, N. Kamel, S. Younes, O. M. Marie, F. R. Waly, A. A. El-Kholy, W. Elmenofy, *Biotechnol. Lett.* **2022**, *44*, 1507–1517.

[35] H. Cai, F. Degliangeli, B. Palitzsch, B. Gerlitzki, H. Kunz, E. Schmitt, R. Fiammengo, U. Westerlind, *Bioorg. Med. Chem.* **2016**, *24*, 1132–1135.

[36] L. Maus, O. Dick, H. Bading, J. P. Spatz, R. Fiammengo, *ACS Nano* **2010**, *4*, 6617–6628.

[37] V. Mangini, V. Maggi, A. Trianni, F. Melle, E. De Luca, A. Pennetta, R. Del Sole, G. Ventura, T. R. I. Cataldi, R. Fiammengo, *Bioconjugate Chem.* **2020**, *31*, 74–81.

[38] F. Degliangeli, P. Kshirsagar, V. Brunetti, P. P. Pompa, R. Fiammengo, *J. Am. Chem. Soc.* **2014**, *136*, 2264–2267.

[39] T. A. Larson, P. P. Joshi, K. Sokolov, *ACS Nano* **2012**, *6*, 9182–9190.

[40] a) D. C. Hone, A. H. Haines, D. A. Russell, *Langmuir* **2003**, *19*, 7141–7144; b) C.-S. Tsai, C.-T. Chen, *ChemPlusChem* **2012**, *77*, 314–322.

[41] Y. Kobayashi, H. Tateno, H. Ogawa, K. Yamamoto, J. Hirabayashi, in *Lectins: Methods and Protocols* (Ed.: J. Hirabayashi), Springer New York, New York, NY, **2014**, pp. 555–577.

[42] M. J. Mattes, *Cancer Immunol. Immunother.* **2005**, *54*, 513–516.

[43] T. Yang, O. K. Baryshnikova, H. Mao, M. A. Holden, P. S. Cremer, *J. Am. Chem. Soc.* **2003**, *125*, 4779–4784.

[44] a) L. Bar, R. Dejeu, R. Lartia, F. Bano, R. P. Richter, L. Coche-Guérente, D. Boturyn, *Anal. Chem.* **2020**, *92*, 5396–5403; b) V. M. Krishnamurthy, L. A. Estroff, G. M. Whitesides, in *Fragment-based Approaches in Drug Discovery*, **2006**, pp. 11–53.

[45] Y. Yoshimura, K. Denda-Nagai, Y. Takahashi, I. Nagashima, H. Shimizu, T. Kishimoto, M. Noji, S. Shichino, Y. Chiba, T. Irimura, *Sci. Rep.* **2019**, *9*, 16641.

[46] K. Lavrsen, C. B. Madsen, M. G. Rasch, A. Woetmann, N. Ødum, U. Mandel, H. Clausen, A. E. Pedersen, H. H. Wandall, *Glycoconjugate J.* **2013**, *30*, 227–236.

[47] a) K. Dobrochaeva, N. Khasbiullina, N. Shilova, N. Antipova, P. Obukhova, T. Ovchinnikova, O. Galanina, O. Blixt, H. Kunz, A. Filatov, Y. Knirel, J. LePendu, S. Khaidukov, N. Bovin, *Mol. Immunol.* **2020**, *120*, 74–82; b) N. Zlocowski, V. Grupe, Y. C. Garay, G. A. Nores, R. D. Lardone, F. J. Irazoqui, *Sci. Rep.* **2019**, *9*, 8097; c) G. F. Springer, C. R. Taylor, D. R. Howard, H. Tegtmeyer, P. R. Desai, S. M. Murthy, B. Felder, E. F. Scanlon, *Cancer* **1985**, *55*, 561–569.

[48] Avery D. Posey, H. Clausen, Carl H. June, *Immunity* **2016**, *45*, 947–948.

[49] K. H. Zou, A. J. O'Malley, L. Mauri, *Circulation* **2007**, *115*, 654–657.

[50] H. Xing, J. Wang, Y. Wang, M. Tong, H. Hu, C. Huang, D. Li, *Gastroenterol. Res. Pract.* **2018**, *2018*, 8704751.

Research Article

Molecular Recognition

F. Corzana,* A. Asín, A. Eguskiza,
E. De Tomi, A. Martín-Carnicero,
M. P. Martínez-Moral, V. Mangini, F. Papi,
C. Bretón, P. Oroz, L. Lagartera, E. Jiménez-
Moreno, A. Avenoza, J. H. Busto, C. Nativi,
J. L. Asensio, R. Hurtado-Guerrero,
J. M. Peregrina, G. Malerba,* A. Martínez,*
R. Fiammengo* ——————— e202407131

Detection of Tumor-Associated Autoantibodies in the Sera of Pancreatic Cancer Patients Using Engineered MUC1 Glycopeptide Nanoparticle Probes
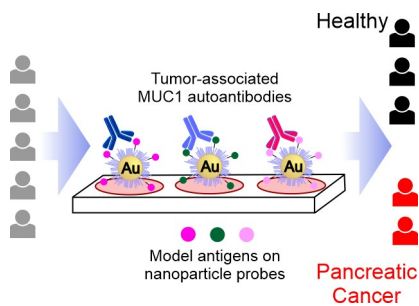
Pancreatic cancer is one of the deadliest cancers worldwide, mainly due to late diagnosis. We describe the development of a diagnostic assay based on the detection of tumor-associated autoantibodies against Mucin-1 (MUC1) in the sera using engineered glycopeptides on nanoparticle probes. The best-discriminating probes show significantly better true and false positive rates than the current clinical biomarkers.